Direct Virtual Torque Control for Doubly Fed Induction Generator Grid Connection

Jihen Arbi, Manel Jebali-Ben Ghorbal, Ilhem Slama-Belkhodja, *Member, IEEE*, and Lotfi Charaabi

***Abstract*—This paper presents a grid-connection control strategy of doubly fed induction generator wind system based on the direct control of both a virtual torque and rotor flux of the generator. This control is achieved with no proportional-integral regulator and requires the measurement of only grid voltages, rotor currents, and rotor position. The same switching table is used for grid synchronization and for running process. A field-programmable-gate-array-based design of the proposed control is developed and tested on a 4-kW experimental prototype. Experimental results are provided to show the effectiveness of the fast and soft grid-connection method developed.**

***Index Terms*—Direct torque control (DTC), doubly fed induction generator (DFIG), field-programmable gate array (FPGA), grid connection, virtual torque, wind energy.**

NOMENCLATURE

$T_{\rm em}$	Electromagnetic torque.
$\vec{\varphi}_s$, $\vec{\varphi}_r$	Stator and rotor flux space vectors.
$\vec{I}_s$, $\vec{I}_r$	Stator and rotor current space vectors.
$\vec{V}_s$, $\vec{V}_r$, $\vec{V}_g$	Stator, rotor, and grid voltage space vectors.
ω_s, ω_r	Synchronous and slip speeds.
R_s, R_r	Stator and rotor resistances.
L_s, L_r	Stator and rotor self-inductances.
M_{sr}	Mutual inductance.
γ	Angle between the stator and the rotor flux space vectors.

I. INTRODUCTION

WIND ENERGY is considered nowadays as one of the most important and promising renewable energy sources [1]. The increasing integration of wind turbine into the grid over the years and, particularly, the growth in medium- and large-size wind farms have reached the point where they have a major impact on the power system [2], [3]. Thus, some countries like Spain, Denmark, and Germany have defined connection requirement of wind farms to the grid and codes in order to integrate wind power generation capacity without affecting the quality and the stability of the power system. One of the main issues of the grid code requirements (GCRs) is the power control and frequency range [4], [5]. For instance, in the wake of grid voltage loss, power has to be ramped up with a specified gradient per minute. This ramp can be achieved in steps by reconnection of a single wind turbine. On the other hand, when grid failures activate protective relays, leading to grid disconnection, the wind turbine can stay in a temporary running-up state. If the fault is cleared and the grid is reestablished before an overspeed situation is reached and before the supervisory control shuts down the wind turbine, a fast synchronization allows rapid reclosing and rapid generator loading [6]. For these reasons, soft and fast synchronization and grid connection at any rotational speed within all the operation range are an important issue with respect to the GCRs.

Wind turbine technology can be divided into fixed speed category (generally with squirrel cage induction generator) and variable speed one (with doubly fed induction generator (DFIG) or synchronous generator) [7], [8]. A variable-speed wind turbine with DFIG (Fig. 1) has the main advantage of a reduced power converter size at around 30% of rated power. The DFIG is connected to the grid directly from the stator side and through a back-to-back converter from the rotor side, providing frequency and voltage control. The control of the rotor-side converter (RsC) allows a decoupled control of active and reactive powers flowing between the stator side and the grid.

Moreover, it achieves a decoupled control of generator torque and the rotor excitation current. The torque control performances are mainstream to reduce mechanical constraints and then to reduce the wear process on the gearbox which has been identified as one of the most critical system components, with a relatively high failure frequency [9].

The most widely used control techniques for the RsC are the field-oriented control (FOC) [10] and the direct control techniques such as direct torque control (DTC), [6], [11], [12] and direct power control (DPC) [13], [14]. The latter techniques do not require current regulators, coordinate transformations, and specific modulations. DTC achieves better steady state and transient torque control conditions, but it presents the drawback of variable switching frequency behavior. However, switching frequency control can be performed using predictive control [15].

The grid-side converter (GsC) can also be controlled by FOC [10], [16], [17] or direct control techniques like the DPC in [18]. As grid connection is performed only with RsC control in the DFIG-based wind system, the GsC will not be detailed in this paper [19].

The present research work will focus on the analysis of the grid-connection and running processes of a DFIG using direct virtual torque control (DVTC) for grid synchronization and DTC for running process.

Manuscript received September 30, 2008; revised April 13, 2009. First published April 28, 2009; current version published September 16, 2009.

The authors are with the Laboratory of Electrical Systems, National School Engineers of Tunis (ENIT), 1002 Tunis, Tunisia (e-mail: jihen_alarbi@yahoo.fr; Maneljebali2001@yahoo.fr; ilhem.slama@enit.rnu.tn; Lotfi.charaabi@enit.rnu.tn).

Color versions of one or more of the figures in this paper are available online at http://ieeexplore.ieee.org.

Digital Object Identifier 10.1109/TIE.2009.2021590

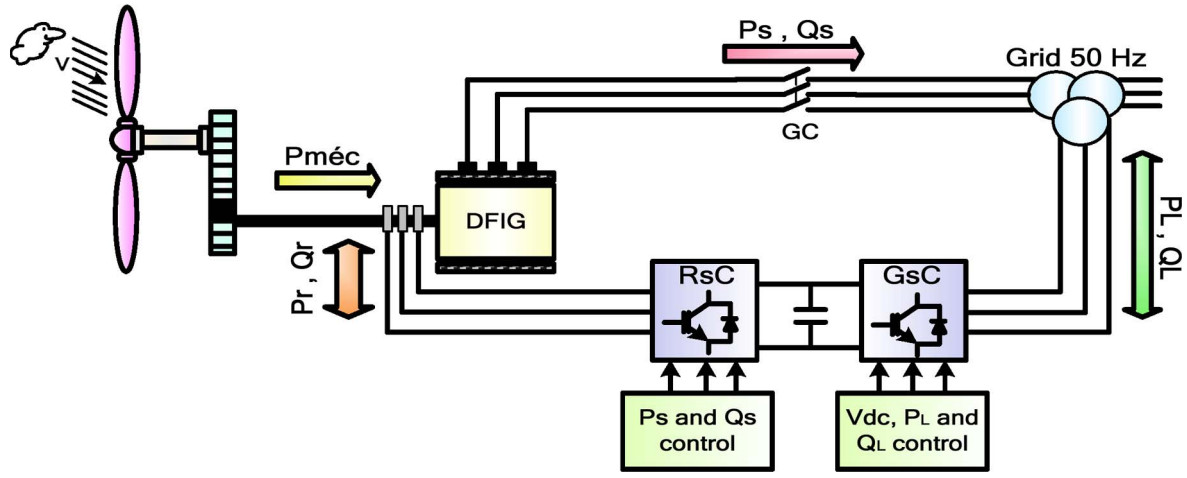

Fig. 1. Studied DFIG-based wind generation system.

The control of the RsC in a DFIG-based wind system has been widely studied and discussed in literature, but only few authors handled the DFIG control for grid-connection process. Before connecting, synchronization between the generated stator voltage vectors with the grid voltage vectors must be performed. The most common approach is based on a vector control method, with a proportional–integral (PI) regulator to achieve magnitude voltage equality and another PI regulator or a phased-locked loop (PLL) control to achieve phase and frequency equality [20]–[22]. In [23], instead of the PLL, the authors propose a turbine pitch angle controller to set the generator frequency equal to the grid one. The DTC approach for grid connection has been presented in [6]. The switching control before and after connecting is easy since the same DTC switching table is used in both cases. Nevertheless, the proposed strategy requires three PI regulators, rotor position and currents, and both stator and grid voltage measurements.

This paper presents a control strategy based on the direct control of a virtual torque for grid connection and on a DTC for running process, with the same DTC switching table like in [6], but no PI regulator is used and only grid voltage, rotor current, and rotor position measurements are needed.

This paper is organized as follows. In Section II, the principles of DTC control and DVTC are presented. In Section III, field-programmable gate-array (FPGA) design and implementation details are developed. Evaluation results are provided to demonstrate the effectiveness of the proposed grid-connection control scheme in Section IV. Conclusions are drawn in Section V.

II. DVTC for DFIG Grid Connection

A. DTC in Grid-Connected Mode

In grid-connected mode, the DTC is applied to the RsC [24]. The DTC for DFIG is based on the same principle as for squirrel cage induction machine [25]. The difference is that, in DTC for DFIG, the rotor flux is regulated, while the DTC for squirrel cage induction machine is based on stator flux regulation. The latter is, indeed, constant in magnitude and frequency as stator windings are directly connected to the grid.

Equation (1) depicts that the electromagnetic torque is a function of stator and rotor flux linkages and the angle γ between them. Hence, the generator torque can be controlled through the control of the magnitude and angle of rotor flux

$$T_{\text{em}} = K \cdot |\vec{\varphi}_r^r| \cdot |\vec{\varphi}_s^r| \cdot \sin\gamma. \tag{1}$$

The constant K is defined as

$$K = \frac{3}{2} p \frac{M_{sr}}{\sigma L_s L_r} \tag{2}$$

where σ is the leakage factor and p is the pole pair number.

Two hysteresis controllers are used to achieve the direct regulation of rotor flux and electromagnetic torque of the DFIG. The relation between the rotor flux and voltage vectors is given by

$$\frac{d\vec{\varphi}r}{dt} = \vec{V}_r - R_r \vec{I}_r. \tag{3}$$

When the effect of the rotor resistance is neglected, (4) can be deduced from (3)

$$\vec{\varphi}_r(k+1) \approx \vec{\varphi}_r(k) + \vec{V}_r T_s \tag{4}$$

where $\vec{\varphi}_r(k)$ and $\vec{\varphi}_r(k+1)$ are the rotor flux vectors at the sampling times $k \cdot T_s$ and $(k+1) \cdot T_s$, respectively.

Relation (4) leads to

$$\Delta\vec{\varphi}_r \approx \vec{V}_r T_s \tag{5}$$

where T_s is the time step of the control algorithm and $\Delta\vec{\varphi}_r$ is the rotor flux variation vector defined by

$$\Delta\vec{\varphi}_r = \vec{\varphi}_r(k+1) - \vec{\varphi}_r(k). \tag{6}$$

Thus, according to (5), the variation of the rotor flux vector is achieved through the application of the appropriate rotor voltage $\vec{V}_r$.

The rotor flux vector rotates in the same direction as the applied rotor voltage vector and with a rotation speed proportional to the rotor voltage magnitude.

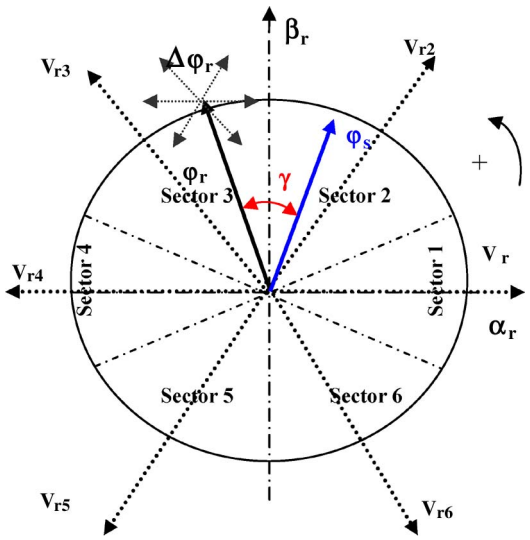

Fig. 2. Rotor voltage vectors and rotor flux control principle.

The DTC strategy is implemented as a lookup table that generates the switching states of the power semiconductors corresponding to the appropriate voltage vector $\vec{V}_r$.

Hence, the choice of the voltage vector depends on the logic outputs of flux and torque controllers and on the position of the flux vector in the $\alpha_r - \beta_r$ rotor plane divided into six sectors (1–6) as shown in Fig. 2.

The DTC optimal switching table is given in Table II in the Appendix.

B. Principle of DVTC

The proposed DVTC is derived from the DTC by substituting the electromagnetic torque $T_{\rm em}$ of the generator by a virtual torque T_v created by the real rotor flux of the machine $\vec{\varphi}_r$ and the so-called grid virtual flux $\vec{\varphi}_g$ which will be defined further in this section. The grid virtual flux $\vec{\varphi}_g$ substitutes, in its turn, the generator stator flux as given by (7). Indeed, $\vec{\varphi}_g$, similar to $\vec{\varphi}_s$ in grid-connected mode, is constant in magnitude and frequency. The grid virtual flux vector is defined as follows:

$$\frac{d\vec{\varphi}_g}{dt} = \vec{V}_g. \tag{7}$$

Its phase θ_g and magnitude $|\vec{\varphi}_g|$ in the grid stationary reference frame $\alpha_g - \beta_g$ are given by

$$\theta_g = \arctan\left(\frac{V_{g_{\beta_g}}}{V_{g_{\alpha_g}}}\right) - \frac{\pi}{2} \tag{8}$$

$$|\vec{\varphi}_g| = \frac{|\vec{V}_g|}{\omega_s} \tag{9}$$

where $V_{g_{\alpha_g}}$ and $V_{g_{\beta_g}}$ are the grid voltage vector $(\vec{V}_g)$ components in $\alpha_g - \beta_g$. The grid voltage vector $\vec{V}_g$ rotates at the grid pulsation ω_s in $\alpha_g - \beta_g$; thus,

$$\omega_s = \frac{d\theta_g}{dt}. \tag{10}$$

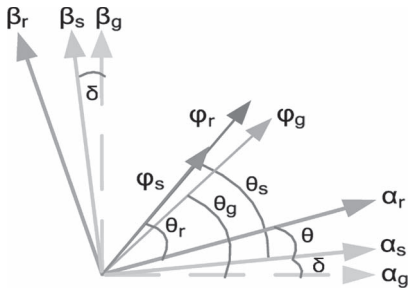

Fig. 3. Stator, rotor, and virtual grid flux vectors.

The virtual torque is then defined as

$$T_v = K\left|\vec{\varphi}_g^{\,r}\right| |\vec{\varphi}_r^{\,r}| \sin\delta \tag{11}$$

where $\vec{\varphi}_g^{\,r}$ and $\vec{\varphi}_r^{\,r}$ are the defined flux vectors in the rotor reference frame $\alpha_r - \beta_r$ and δ is the angle between them. Fig. 3 shows the different vectors where $\alpha_r - \beta_r$, $\alpha_s - \beta_s$, and $\alpha_g - \beta_g$ are rotor, stator, and grid reference frames, respectively.

According to (11), the virtual torque control is achieved through the control of the generator rotor flux in the same way as the electromagnetic torque control in the DTC of grid-connected mode.

Note that the constant K, although dependent on machine parameters, does not affect the virtual torque regulation as T_v will be kept equal to zero during synchronization process. In addition, based on (11), regulating virtual torque to zero implies imposing $\sin\delta = 0$, independently on the value of the constant K.

C. DVTC for DFIG Grid Connection

Connection of DFIG to the grid terminals requires the adjustment of stator voltage to be synchronized with the grid voltage. The main objective of the RsC control, in the grid-connection process, is meeting the synchronization conditions.

These conditions are equality in phase, frequency, and magnitude between the grid and stator voltage vectors ($\vec{V}_g$ and $\vec{V}_s$, respectively).

The following equations recall the relation between stator voltage and flux vectors:

$$\frac{d\vec{\varphi}_s}{dt} = \vec{V}_s \tag{12}$$

$$\theta_s = \arctan\left(\frac{V_{s_{\beta_s}}}{V_{s_{\alpha_s}}}\right) - \frac{\pi}{2}. \tag{13}$$

Indeed, the stator flux vector phase in the stator reference frame $\alpha_s - \beta_s$ shown in Fig. 2 is expressed in (13) as a function of stator voltage components.

According to (7) and (12), equality in phase and frequency between grid and stator voltage vectors is equivalent to the equality in phase and frequency between grid virtual flux vector $\vec{\varphi}_g$ and stator flux vector $\vec{\varphi}_s$.

Making use of the phasor diagram in Fig. 2, equality in phase and frequency between the two voltage vectors, which are, as aforementioned, the first two synchronization conditions, can

be met through bringing to collinearity virtual grid flux and stator flux vectors by eliminating the angle δ between them.

Furthermore, before grid connection, in the no-load mode, the DFIG develops no torque as the stator windings are open. This implies that $\vec{\varphi}_s$ and $\vec{\varphi}_r$ are collinear.

Thus, moving the stator flux direction to be collinear to the virtual grid flux direction is actually equivalent to moving the rotor flux vector to be collinear to the virtual grid flux vector.

Based on the aforementioned analysis and according to (11), one can state that the grid virtual flux and stator flux vectors are collinear when the virtual torque T_v is null. This condition is guaranteed through the torque control loop of the proposed DVTC by imposing a reference virtual torque T_{v_ref} equal to zero.

One of the important features of the proposed DVTC is that, the way it has been developed, its corresponding optimal switching table is, in fact, the same as that of the DTC.

Furthermore, all DVTC algorithm modules remain unchanged with regard to the DTC. Only torque estimator and external references for control loops have to be changed when switching from the DVTC in no-load mode to DTC in grid-connected mode.

However, the switching from a virtual torque estimator to an electromagnetic torque estimator does not affect the performance of the control system. This is due to the fact that during the transition between the no-load and grid-connected modes, both torques (T_v and T_{em}) are equal to zero.

In fact, on the one hand, before grid connection, T_v is null in order to satisfy the first two synchronization conditions as previously explained. On the other hand, the generator is not immediately loaded when the stator terminals are connected to the grid. This implies that, in the first seconds after the grid connection, the electromagnetic torque T_{em} is still null.

The third condition for the synchronization of grid and stator voltages is equality in magnitude between them.

The amplitude of the induced stator voltage is indirectly controlled through adjusting the rotor excitation by means of the rotor flux control loop of the proposed DVTC.

In fact, the appropriate rotor flux reference is imposed to the rotor flux hysteresis controller in order to guarantee the required stator voltage amplitude. In this way, the proposed DVTC achieves a decoupled control of the instantaneous angle and amplitude of the stator voltage vector through the torque and flux control loops, respectively.

In the following, we detail the computation method of the required rotor flux reference. It is based mainly on the no-load mode model of the generator.

The dynamic machine equations with a complex representation are given in the following, in a synchronous reference frame:

$$\vec{V}_s = R_s\vec{I}_s + \frac{d\vec{\varphi}_s}{dt} + j\omega_s\vec{\varphi}_s \tag{14}$$

$$\vec{V}_r = R_r\vec{I}_r + \frac{d\vec{\varphi}_r}{dt} + j\omega_r\vec{\varphi}_r \tag{15}$$

$$\vec{\varphi}_s = L_s\vec{I}_s + M_{sr}\vec{I}_r \tag{16}$$

$$\vec{\varphi}_r = L_r\vec{I}_r + M_{sr}\vec{I}_s. \tag{17}$$

In no-load operation, the stator terminals are open; thus,

$$\vec{I}_s = 0. \tag{18}$$

In steady-state operation, (14), (16), and (18) become

$$\vec{V}_s = j\omega_s\vec{\varphi}_s \tag{19}$$

$$\vec{\varphi}_s = M_{sr}\vec{I}_r \tag{20}$$

$$\vec{\varphi}_r = L_r\vec{I}_r. \tag{21}$$

Substituting (19) and (20) into (21), the reference of rotor flux amplitude is given by

$$|\vec{\varphi}_r|_{\mathrm{ref}} = \frac{L_r}{M_{sr}}\frac{|\vec{V}_s|_{\mathrm{ref}}}{\omega_s}. \tag{22}$$

The rotor flux command is then calculated through the estimation of grid voltage magnitude and pulsation using only measured grid voltages.

The overall control strategy scheme is shown in Fig. 4.

The equations used for the estimation of rotor flux components in rotor reference frame are given as follows:

$$\begin{aligned}\varphi_{r\alpha_r} &= L_r \cdot i_{r\alpha_r} + M_{sr} \cdot [i_{s\alpha} \cdot \cos(\theta) + i_{s\beta} \cdot \sin(\theta)]\\ \varphi_{r\beta_r} &= L_r \cdot i_{r\beta_r} + M_{sr} \cdot [i_{s\beta} \cdot \cos(\theta) - i_{s\alpha} \cdot \sin(\theta)]\end{aligned} \tag{23}$$

where θ is the rotor position provided by an incremental encoder. The grid virtual flux components are estimated using (8) and (9) and polar to Cartesian transformation based on Cordic algorithm [26].

The rotor flux command equation given in (22) depends on machine parameters. However, this parameter dependence is low compared to the FOC where PI regulators are tuned using more machine parameters, including rotor and stator resistances like in [23], for instance.

Furthermore, as the rotor and grid virtual flux are both rotating at the slip frequency in the rotor reference frame, the switching frequency is reduced and thus the switching losses. However, the DVTC performances can be further improved by including switching frequency control [14].

At this stage, the main features of the developed DVTC can be cited as follows.

1) Only grid feedback is needed for the control of the stator voltage amplitude as given by (22). Thus, the measurement of stator voltages is useless here. This is not the case for the majority of control strategies for grid connection of DFIG already presented in the literature.
2) The control is further simplified by the elimination of PI regulators with regard to the previously presented DTC [6] and FOC for grid connection of DFIG. Obviously, these regulators make the controls more complicated because of the difficulty related to their parameter tuning which, in some cases, is done intuitively. In the proposed DVTC, only two hysteresis controllers are used.

Further important features will be pointed out in the next sections where both simulation and experimental results will be presented and discussed.

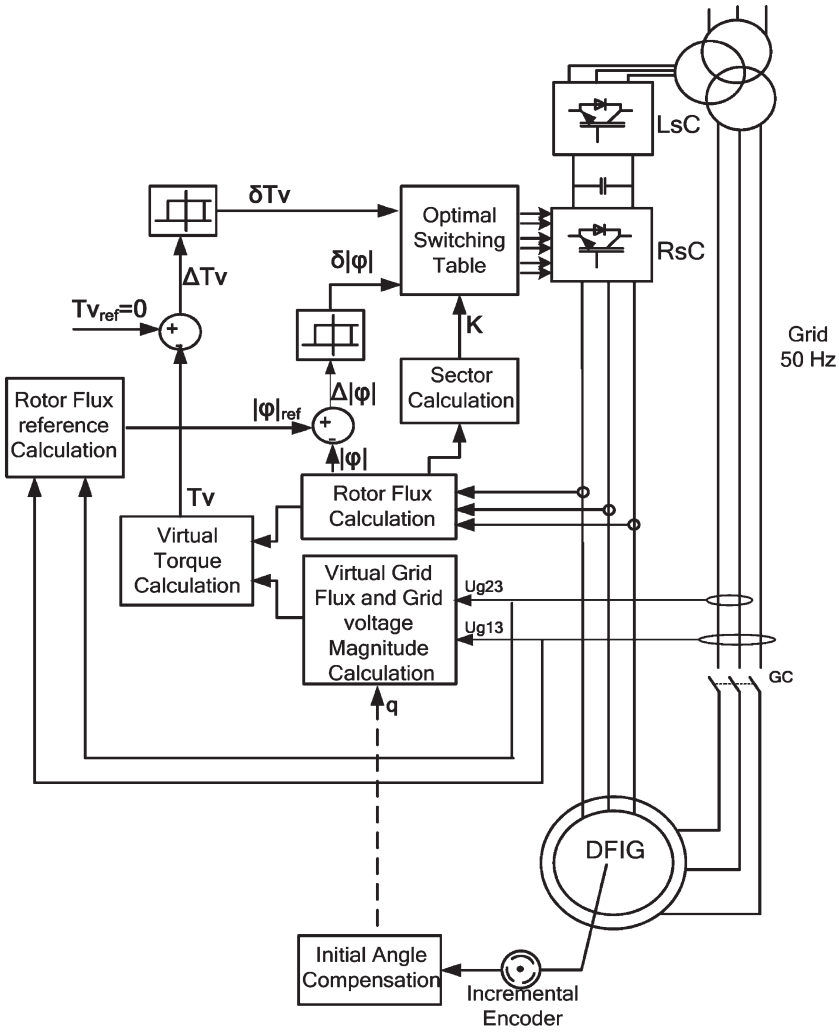

Fig. 4. DVTC scheme for DFIG grid connection.

III. FPGA Design and Control Algorithm Implementation

With respect to control algorithm requirements, a system-on-module approach, combined with FPGA-based intellectual property (IP), is used for architecture development.

After the specification of the algorithm, we propose to develop a custom modular architecture for the DVTC to be implemented in an FPGA device. This architecture is developed following a design methodology that allows the adequation between control performances and hardware implementation constraints [27]. The control algorithm is implemented in FPGA as a mix of elementary IP-core functions according to the algorithmic decomposition, so that the resulted architecture is built from a library of IP-core modules [28]. Each module is described from the hardware level using structural VHDL.

The control architecture is implemented in a low-cost Xilinx SPARTAN3 XCS400PQ208 FPGA target device containing 400 000 logical gates and a 50-MHz oscillator.

The control unit "global sequencer" initiates the algorithm by generating a suitable timing schedule to control several modules. Fig. 5 shows the top view of the module disposition of the DVTC architecture on the FPGA device. The label of each module in the figure indicates the activation order generated by the global sequencer.

The whole execution time of the DVTC is only 5.92 μs. The implementation results are given in Table I. Note that these execution performances are mainly due to the fast computation capabilities of FPGAs, which represent one of their major features.

IV. Experimental Results

The emulation of the wind turbine is done by means of a 7.5-kW/3000-r/min induction motor under speed control using a Danfoss VLT5011 frequency converter. The DFIG is a 4.5-kW/1500-r/min wound rotor induction machine. The back-to-back converters connecting the DFIG to the grid in the rotor side are two ac/dc insulated-gate-bipolar-transistor-based converters from SEMIKRON. An autotransformer allows a safe dc voltage installation in the starting. The machine parameters are given in Table III in the Appendix. Hall-effect sensors (LEM 25NA) are used for current measuring, and Tektronix differential probes (P5200) are used for voltages. An interface board (ARCU3I) allows the voltage level adaptation between the LEM sensors and the analog-to-digital (AD) conversion interface (2.5 V/20 A). Two 12-b circuits (AD9221) are used

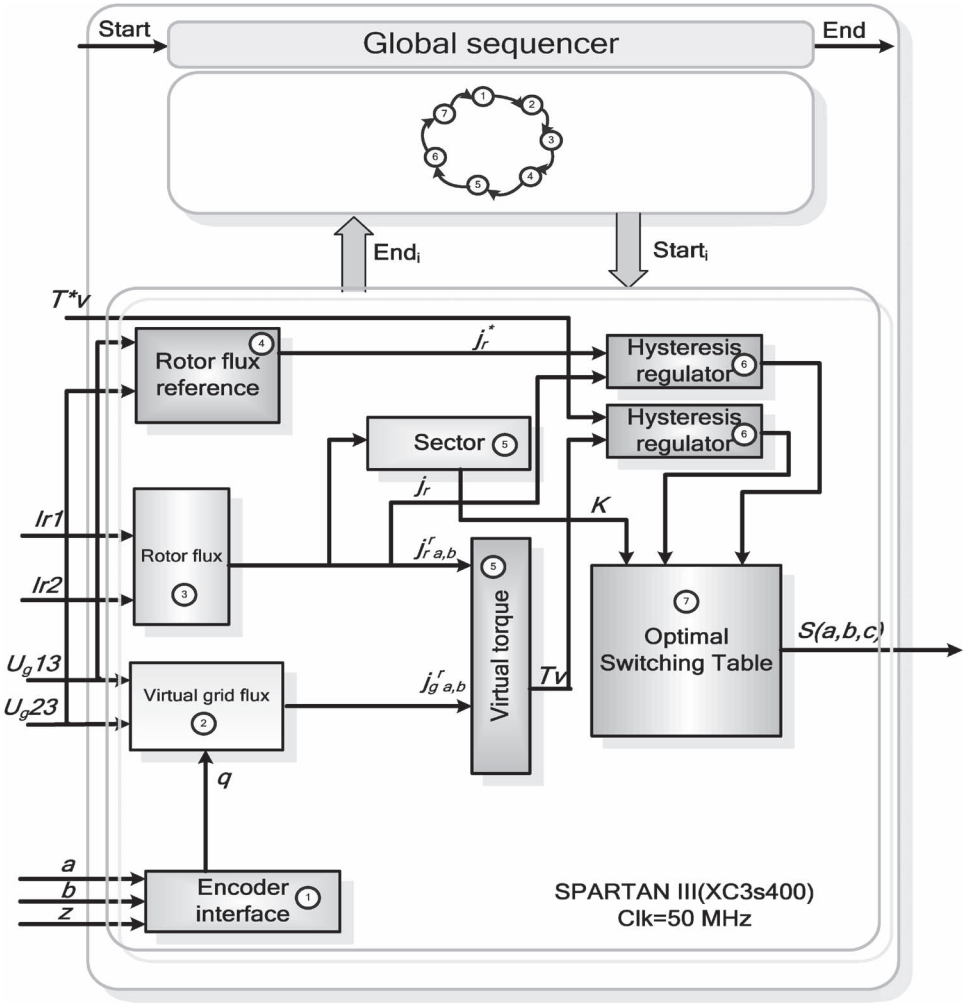

Fig. 5. DVTC modular architecture for FPGA implementation.

TABLE I
FPGA TIME/AREA PERFORMANCES OF DVTC FOR DFIG GRID CONNECTION

Module	Latency	Computation time
Grid virtual flux	40	T_1=0.8μs
Rotor Flux	44	T_2=0.88μs
Sector	4	T_3=0.08μs
Virtual torque	8	T_4=0.16μs
Hysteresis controller	4	T_5=0.8μs
Optimal switching table	4	T_6=0.8μs
AD interface		T_7=T_{AD}= 2.4μs
Execution time T_{ex}= T_1+ T_2+ T_3+ T_4+ T_5+ T_6+ T_7		T_{ex}= 5.92μs
Consumed resources		56%

for AD conversion of measured rotor currents and grid voltages with 100-μs sampling period. A 10-b incremental encoder is used to measure the DFIG rotor mechanical position. A voltage-source inverter (VSI) interface board and a host PC connected with the FPGA via serial interface are used as well. This platform is modular and can be extended to more than one FPGA (Fig. 6). The AD conversion time is equal to 2.4 μs. The VSI is set with a 3-μs dead time for the sake of security. Fig. 7 shows the waveforms of the stator and grid voltages at the grid-connection instant. The two curves are in close agreement in phase, frequency, and magnitude. The grid-connection process can be done in a safe way through closing the GC switch (Fig. 1).

As explained in Section II, to eliminate any phase difference between stator and grid voltages, the virtual torque T_v must be imposed equal to zero. Thus, when the virtual torque is different from zero, the two voltage vectors are no more collinear. A phase difference is then created between them. This result has been confirmed both by simulation and experiments as shown in Fig. 8. Simulations are performed with MATLAB-Simulink for the control associated to PSIM from POWERSYS for the power system.

In fact, a torque step is applied to the torque control loop of the proposed DTC from 0.2 to 0 p.u. It is obvious how the virtual torque affects the phase difference between the stator and grid voltages. When the virtual torque is equal to 0.2 p.u., the stator voltage is leading the grid voltage. When the torque step is applied, the virtual torque is forced to be null. Thus, the two waveforms coincide.

The control response is fast, as expected. The DFIG grid connection is smooth. This is confirmed through Fig. 9. Indeed, no current inrush has been provoked at the connection instant.

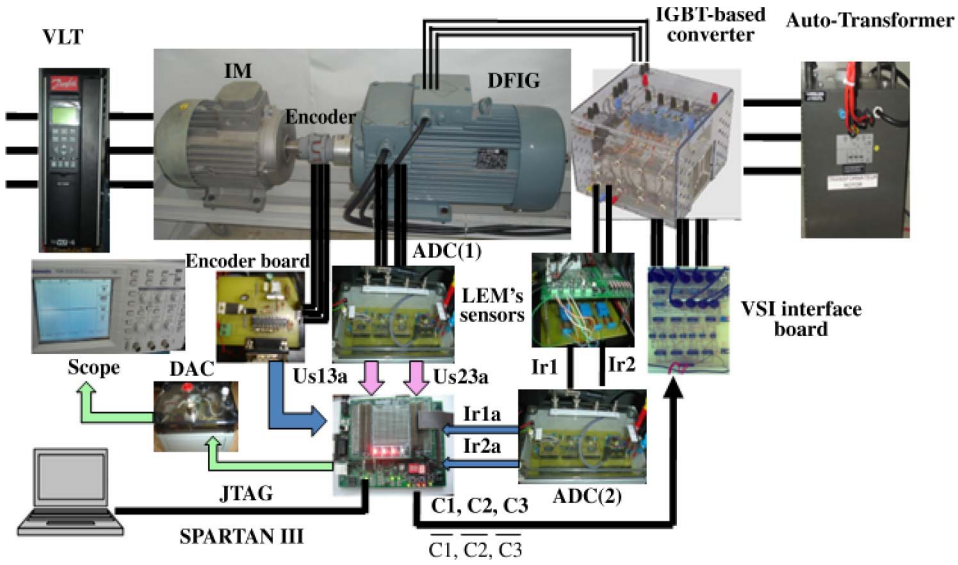

Fig. 6. Experimental laboratory setup.

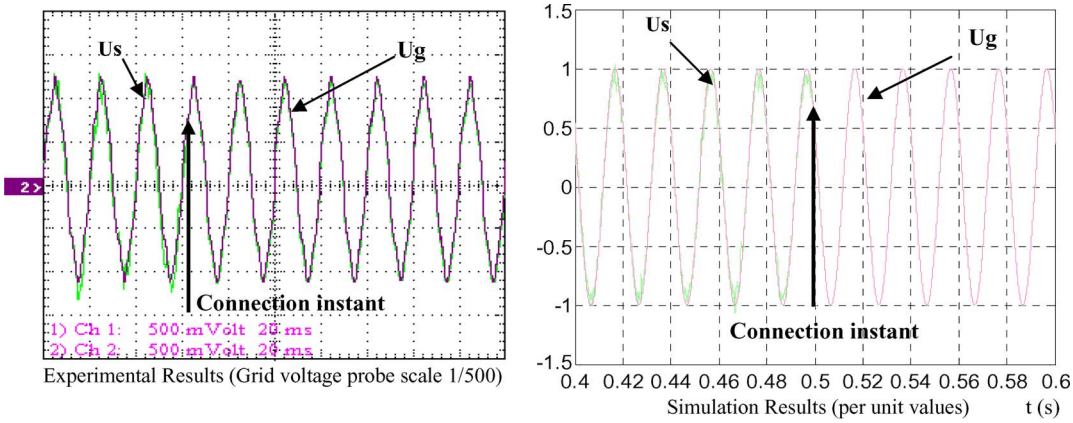

Fig. 7. Grid (U_g) and stator (U_s) line-to-line voltages at grid-connection instant.

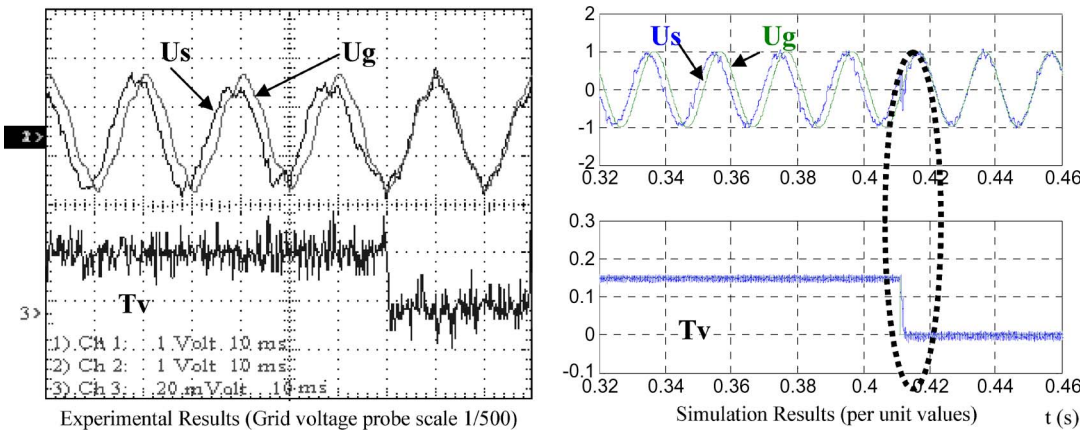

Fig. 8. Grid line-to-line voltage (U_g) and stator line-to-line voltage (U_s) and virtual torque (T_v).

Fig. 10 shows the stator voltage, grid voltage, and rotor current for two different angular speeds ($N1 = 900$ r/min and $N2 = 1260$ r/min) of the DFIG. The decoupling between stator and rotor frequencies, offered by the back-to-back converter connected to the rotor of the DFIG, allows the grid connection for different speeds. Indeed, for both angular velocities $N1$ [Fig. 10(a)] and $N2$ [Fig. 10(b)], the synchronization between stator and grid voltages is kept. This represents one of the numerous advantages and flexibilities of the DFIG-based wind system.

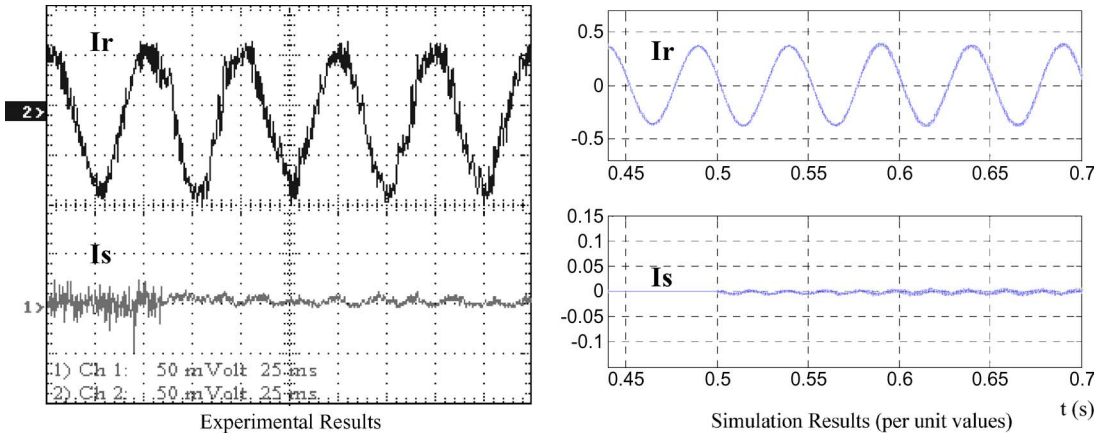

Fig. 9. Rotor and stator currents at the grid-connection moment.

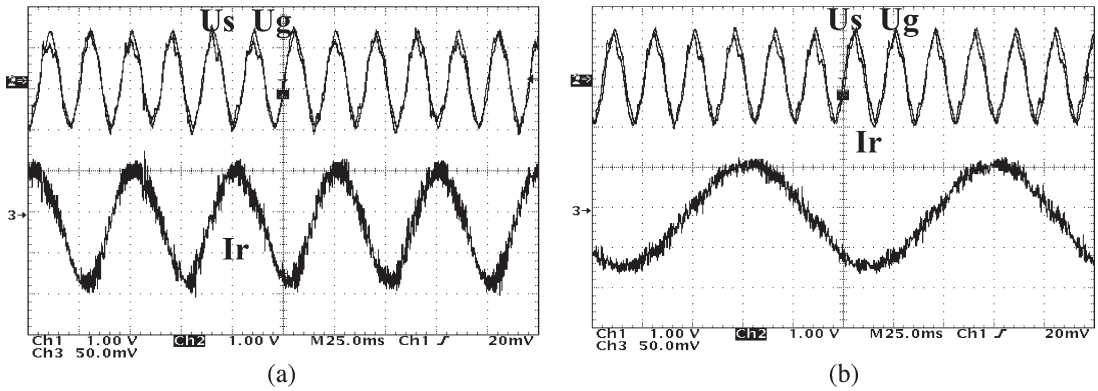

Fig. 10. Experimental results of grid and stator voltages and rotor current of DTC for DFIG grid connection at two different speeds. (a) $N1 = 900$ r/min. (b) $N2 = 1260$ r/min.

V. Transition From the No-Load Mode to the Grid-Connected Mode

For the sake of simplification, we adopt the following notation.

Mode 1) Operation mode during the synchronization process before connection of the generator stator terminals to the grid previously noted as the no-load mode.

Mode 2) Operation mode with the stator of the DFIG connected to the grid previously defined as the grid-connected mode.

The previous analysis allows one to state that the transition from mode 1 to mode 2 requires the following.

1) First, the switching from the virtual torque estimator needed for the DVTC in mode 1 to the generator electromagnetic torque used in the DTC algorithm of mode 2.
2) Second, the switching from the rotor flux reference calculation based on (22) in mode 1 to the one based on the stator reactive power command as mentioned in Section II.

Fig. 11 shows the switching process. One can note that the change in the torque reference of torque control loop is seen by the overall control as a reference step independently of the nature of the estimated torque.

In the same way, the switching from the rotor reference calculation of mode 1 to the one of mode 2 is equivalent to the rotor flux reference step.

Furthermore, the rotor flux estimator is naturally the same for the two modes.

Simulations were carried out under MATLAB-Simulink and PSIM environments in order to prove the effectiveness of the proposed overall control system.

In Fig. 12, the grid connection is done at $t = 0.5$ s. At $t = 0.505$ s, a torque reference step ($T_{\mathrm{em\_ref}} = 0.6$ p.u. where generator nominal torque is the base value) is applied to the torque control loop.

Between $t = 0.5$ s and $t = 0.505$ s, the stator current and the generator torque are both equal to zero as the generator is not loaded yet [Fig. 12(a)].

At $t = 0.505$ s, the control switches from the virtual torque estimator to the electromagnetic torque one. It must be pointed out here that at that moment, both torques are equal to zero. This is the reason why the switching is done smoothly without affecting the performances of the control system.

Fig. 12(c) shows the rotor currents. Until $t = 0.505$ s, these are, in fact, the magnetizing currents with the appropriate amplitude and frequency that guarantee the desired amplitude and frequency of the induced stator voltages. In Fig. 12(c), a zoom of stator currents is shown to emphasize the soft grid connection and mode transition through the absence of any current inrush.

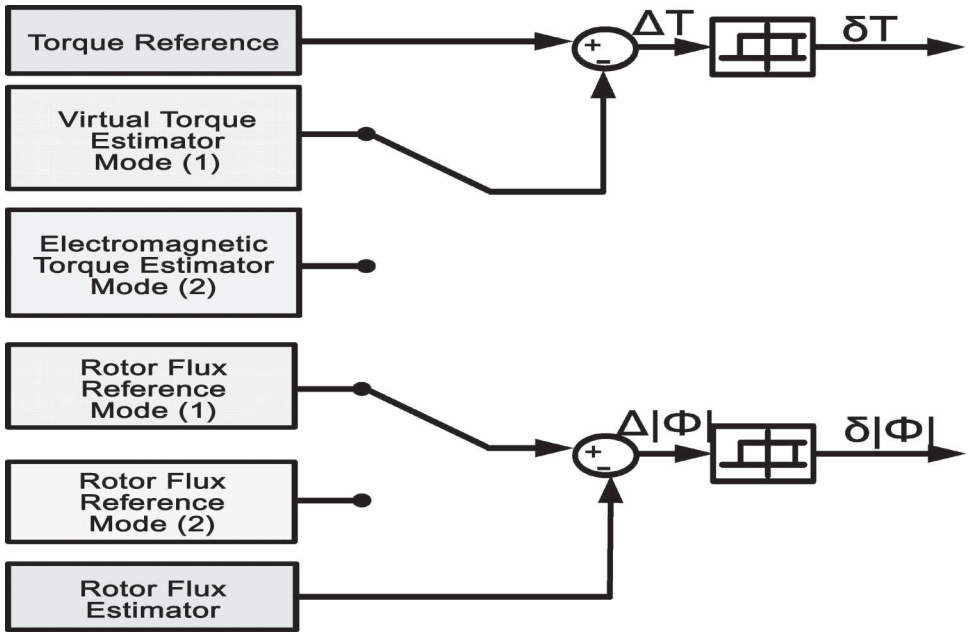

Fig. 11. Principle of transition from no-load mode to grid-connection mode.

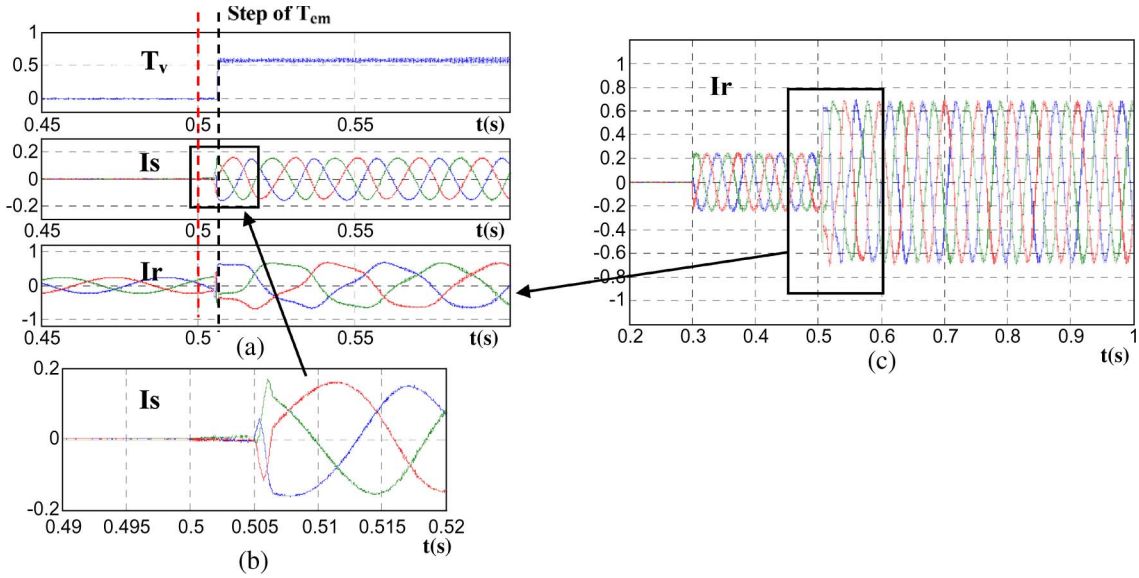

Fig. 12. Simulation results of no-load mode to grid-connection mode transition.

The smooth behavior is noticed as well on the torque estimator [Fig. 12(a)] and rotor currents [Fig. 12(b)].

VI. Conclusion

A DVTC for the grid connection of DFIG to the grid has been proposed. This new control method is based on the control of the generator rotor flux and newly defined virtual torque in order to meet synchronization conditions between grid and stator voltages.

The main features of the proposed DVTC can be summarized as follows: 1) The control needs only stator voltage feedback as the stator voltages are not needed; 2) the control is simple since no PI regulators are used. Thus, problems related to parameter tuning and machine parameter dependence are eliminated; and 3) the grid connection can be achieved at any rotational speed and is done softly without any current inrush, thus resulting in safe conditions for the both the generator and the grid to which it will be connected.

Relevant experimental results in close agreement with their simulation counterparts have been presented to show the benefits and effectiveness of the proposed control method.

Furthermore, authors have shown that the transition from DVTC in the no-load mode to the DTC of the running mode can be done in a smooth way, taking advantage of the good dynamics and the fast response time of direct controls. This constitutes a complete control system based on the DTC that allows the control of the RsC in the two operating modes, namely, mode 1 before grid connection and mode 2 after grid connection, and manages efficiently the transition between the two modes.

APPENDIX

TABLE II
DTC AND DVTC OPTIMAL SWITCHING TABLE

τ_φ	1	1	0	0
τ_c	1	0	1	0
K=1	V_{r2}	V_{r6}	V_{r3}	V_{r5}
K=2	V_{r3}	V_{r1}	V_{r4}	V_{r6}
K=3	V_{r4}	V_{r2}	V_{r5}	V_{r1}
K=4	V_{r5}	V_{r3}	V_{r6}	V_{r2}
K=5	V_{r6}	V_{r4}	V_{r1}	V_{r3}
K=6	V_{r1}	V_{r5}	V_{r2}	V_{r4}

TABLE III
MACHINE PARAMETERS

		DFIG	IM
P_N	rated power	4 kW	7.5 kW
$U_{N,s}$	rated stator voltage	690 V (delta)	380V (delta)
$U_{max,r}$	rated rotor voltage	130 V (star)	
f_N	rated stator frequency	50 Hz	50 Hz
n_N	nominal speed	1435 rpm	2880 rpm
$I_{N,s}$	rated stator current	4.6 A	15.6 A
$I_{N,r}$	rated rotor current	19 A	
p	poles pairs	2	1

REFERENCES

[1] L. Jodziewicz, "Environmental and sitting status and needs of 20% electricity from wind power," in *Conf. IEEE Power Energy Soc. Gen. Meeting—Convers. Del. Elect. Energy 21st Century*, Jul. 2008, pp. 1–6.

[2] J. Hu, Y. He, L. Xu, and B. W. Williams, "Improved control of DFIG systems during network unbalance using PI–R current regulators," *IEEE Trans. Ind. Electron.*, vol. 56, no. 2, pp. 439–451, Feb. 2009.

[3] S. Alepuz, S. Busquets-Monge, J. Bordonau, J. Gago, D. Gonzalez, and J. Balcells, "Interfacing renewable energy sources to the utility grid using a three-level inverter," *IEEE Trans. Ind. Electron.*, vol. 53, no. 5, pp. 1504–1511, Oct. 2006.

[4] B. Alboyaci and B. Dursun, "Grid connection requirements for wind turbine systems in selected countries. Comparison to Turkey," *Elect. Power Quality Utilization Mag.*, vol. 3, no. 2, Jun. 2008. [Online]. Available: http://www.scribd.com/doc/

[5] G. Joos, "Turbine generator low voltage ride through requirements and solutions," in *Conf. Rec. IEEE Power Energy Soc. Gen. Meeting—Convers. Del. Elect. Energy 21st Century*, Jul. 2008, pp. 1–7.

[6] S. A. Gomez and J. L. R. Amenedo, "Grid synchronisation of doubly fed induction generators using direct torque control," in *Proc. IEEE IECON Conf.*, Nov. 2002, pp. 3338–3343. CD-ROM.

[7] J. M. Carrasco, L. G. Franquelo, J. T. Bialasiewicz, E. Galvan, R. C. Portillo Guisado, M. A. M. Prats, J. I. Leon, and N. Moreno-Alfonso, "Electronic systems for the grid integration of renewable energy sources: A survey," *IEEE Trans. Ind. Electron.*, vol. 53, no. 4, pp. 1002–1016, Jun. 2006.

[8] M. Malinowski, S. Stynski, W. Kolomyjski, and M. P. Kazmierkowski, "Control of three-level PWM converter applied to variable-speed-type turbines," *IEEE Trans. Ind. Electron.*, vol. 56, no. 1, pp. 69–77, Jan. 2009.

[9] J. Ribrant and L. Bertling, "Survey of failures in wind power systems with focus on Swedish wind power plants during 1997–2005," in *Conf. Rec. IEEE Power Eng. Soc. Gen. Meeting*, Jun. 2007, pp. 1–8.

[10] R. Pena, J. C. Clare, and G. M. Asher, "Doubly fed induction generator using back-to-back PWM converters and its application to variable-speed wind-energy generation," *Proc. Inst. Elect. Eng.—Electr. Power Appl.*, vol. 143, no. 3, pp. 231–241, May 1996.

[11] J. Arbi, I. Slama-Belkhodja, and S. A. Gomez, "Control of a DFIG-based wind system in presence of large grid faults: Analysis of voltage ride through capability," in *Proc. IEEE-EPQU*, Barcelona, Spain, Oct. 2007, pp. 1–6.

[12] Z. Liu, O. A. Mohammed, and S. Liu, "A novel direct torque control of doubly-fed induction generator used for variable speed wind power generation," in *Conf. Rec. IEEE Power Eng. Soc. Gen. Meeting*, Jun. 2007, pp. 1–6.

[13] L. Xu and P. Cartwright, "Direct active and reactive power control of DFIG for wind energy generation," *IEEE Trans. Energy Convers.*, vol. 21, no. 3, pp. 750–758, Sep. 2006.

[14] D. Zhi and L. Xu, "Direct power control of DFIG with constant switching frequency and improved transient performance," *IEEE Trans. Energy Convers.*, vol. 22, no. 1, pp. 110–118, Mar. 2007.

[15] G. Abad, M. A. Rodriguez, and J. Poza, "Two-level VSC based predictive direct torque control of the doubly fed induction machine with reduced torque and flux ripples at low constant switching frequency," *IEEE Trans. Power Electron.*, vol. 23, no. 3, pp. 1050–1061, May 2008.

[16] E. Figueres, G. Garcera, J. Sandia, F. Gonzalez-Espin, and J. C. Rubio, "Sensitivity study of the dynamics of three-phase photovoltaic inverters with an LCL grid filter," *IEEE Trans. Ind. Electron.*, vol. 56, no. 3, pp. 706–717, Mar. 2009.

[17] J. Dannehl, C. Wessels, and F. W. Fuchs, "Limitations of voltage-oriented PI current control of grid-connected PWM rectifiers with LCL filters," *IEEE Trans. Ind. Electron.*, vol. 56, no. 2, pp. 380–388, Feb. 2009.

[18] B. Rueckert and W. Hofmann, "Common mode voltage minimized direct power control of the grid side connected converter in doubly fed induction generators," in *Proc. IEEE-SDEMPED*, Ischia, Italy, Jun. 11–13, 2008, pp. 1455–1459.

[19] F. Blaabjerg, R. Teodorescu, M. Liserre, and A. V. Timbus, "Overview of control and grid synchronization for distributed power generation systems," *IEEE Trans. Ind. Electron.*, vol. 53, no. 5, pp. 1398–1409, Oct. 2006.

[20] P. Jungwoo, L. Kiwook, K. Dongwook, L. Kwangsoo, and P. Jinsoon, "An encoder-free grid synchronization method for a doubly-fed induction generator," in *Proc. EPE Conf.*, Aalborg, Denmark, Sep. 2–5, 2007, pp. 1–6.

[21] Z. Xueguang, X. Dianguo, L. Yongqiang, and M. Hongfei, "Study on stagewise control of connecting DFIG to the grid," in *Proc. IEEE-IPEMC*, Shanghai, China, Aug. 14–16, 2006, pp. 1–5.

[22] G. Iwanski and W. Koczara, "Grid connection to stand alone transitions of slip ring induction generator during grid faults," in *Conf. Rec. IEEE-IPEMC*, Shanghai, China, Aug. 14–16, 2006, pp. 1–5.

[23] A. G. Abo-Khalil, L. Dong-Choon, and L. Se-Hyun, "Grid connection of doubly-fed induction generators in wind energy conversion system," in *Conf. Rec. IEEE-IPEMC*, Shanghai, China, Aug. 2006, pp. 1–5.

[24] S. Arnaltes, J. C. Burgos, and J. L. Rodriguez-Amenedo, "Direct torque control of a doubly-fed induction generator for variable speed wind turbines," *Elect. Power Compon. Syst.*, vol. 30, no. 2, pp. 199–216, Feb. 2002.

[25] I. Takahashi and T. Nouuchi, "A new quick-response and high-efficiency control strategy of an induction motor," *IEEE Trans. Ind. Appl.*, vol. IA-22, no. 5, pp. 820–827, Sep./Oct. 1986.

[26] R. Andraka, *A Survey of CORDIC Algorithms for FPGA Based Computers*. North Kingstown, RI: Consulting Group, Inc. [Online]. Available: www.fpga-guru.com/files/crdcsrvy.pdf

[27] M.-W. Naouar, E. Monmasson, A. Naassani, I. Slama-Belkhodja, and N. Patin, "FPGA-based current controllers for AC machine drives—A review," *IEEE Trans. Ind. Electron.*, vol. 54, no. 4, pp. 1907–1946, Aug. 2007.

[28] E. Monmasson and M. N. Cirstea, "FPGA design methodology for industrial control systems—A review," *IEEE Trans. Ind. Electron.*, vol. 54, no. 4, pp. 1824–1842, Aug. 2007.

Jihen Arbi was born in Tunisia in 1978. She received the B.S., M.S., and Ph.D. degrees in electrical engineering from the Ecole Nationale d'Ingénieurs de Tunis (ENIT), Tunis, Tunisia, in 2002, 2003, and 2008, respectively.

She is currently a permanent Researcher in the Laboratory of Electrical Systems, ENIT. Her main research interests are in the areas of ac machine drives and variable-speed wind energy systems.

Manel Jebali-Ben Ghorbal was born in Nabeul, Tunisia, in 1983. She received the B.S. and M.S. degrees in electrical engineering from the Ecole Nationale d'Ingénieurs de Tunis (ENIT), Tunis, Tunisia, in 2007 and 2008, respectively, where she is currently working toward the Ph.D. degree in electrical engineering in the Laboratory of Electrical Systems.

Her current research interests include machine drives, control and operation of doubly fed induction generators for wind energy generation, and field-programmable-gate-array-based controllers.

Ilhem Slama-Belkhodja (M'08) received the B.S. degree in electrical engineering from the Ecole Nationale Supérieure d'Electrotechnique, d'Electronique, d'Informatique, d'Hydraulique et des Télécommunications (ENSEEIHT)–Institut National Polytechnique de Toulouse (INPT), Toulouse, France, in 1983, the Ph.D. degree from the INPT in 1985, and the Doctorat d'Etat from the Ecole Nationale d'Ingénieurs de Tunis (ENIT), Tunis, Tunisia, in 1997.

She is currently a Professor and the Head of the Laboratory of Electrical Systems, ENIT. Her current research activities are in the field of fault-tolerant control for electrical drives.

Lotfi Charaabi was born in Tunisia in 1977. He received the B.S. and M.S. degrees in telecommunication from the Ecole Nationale d'Ingénieurs de Tunis (ENIT), Tunis, Tunisia, in 2001 and 2002, respectively, and the Ph.D. degree in electrical engineering jointly from ENIT and the Ecole Normale Supérieure de Cachan, Cachan, France, in 2006.

He is currently a Researcher in the Laboratory of Electrical Systems, ENIT. His main research interests include embedded systems, system on chip, and design and integration of electrical system algorithms on field-programmable gate arrays.